ACS APPLIED MATERIALS & INTERFACES

Research Article

www.acsami.org

Highly Flexible Freestanding Porous Carbon Nanofibers for Electrodes Materials of High-Performance All-Carbon Supercapacitors

Ying Liu, Jinyuan Zhou, Lulu Chen, Peng Zhang, Wenbin Fu, Hao Zhao, Yufang Ma, Xiaojun Pan,* Zhenxing Zhang, Weihua Han, and Erqing Xie*

School of Physical Science and Technology, Lanzhou University, Lanzhou 730000, China

ABSTRACT: Highly flexible porous carbon nanofibers (P-CNFs) were fabricated by electrospining technique combining with metal ion-assistant acid corrosion process. The resultant fibers display high conductivity and outstanding mechanical flexibility, whereas little change in their resistance can be observed under repeatedly bending, even to 180°. Further results indicate that the improved flexibility of P-CNFs can be due to the high graphitization degree caused by Co ions. In view of electrode materials for high-performance supercapacitors, this type of porous nanostructure and high graphitization degree could synergistically facilitate the electrolyte ion diffusion and electron transportation. In the three electrodes testing system, the resultant P-CNFs electrodes can exhibit a specific capacitance of 104.5 F g^{-1} (0.2 A g^{-1}), high rate capability (remain 56.5% at 10 A g^{-1}), and capacitance retention of ~94% after 2000 cycles. Furthermore, the assembled symmetric supercapacitors showed a high flexibility and can deliver an energy density of 3.22 Wh kg^{-1} at power density of 600 W kg^{-1}. This work might open a way to improve the mechanical properties of carbon fibers and suggests that this type of freestanding P-CNFs be used as effective electrode materials for flexible all-carbon supercapacitors.

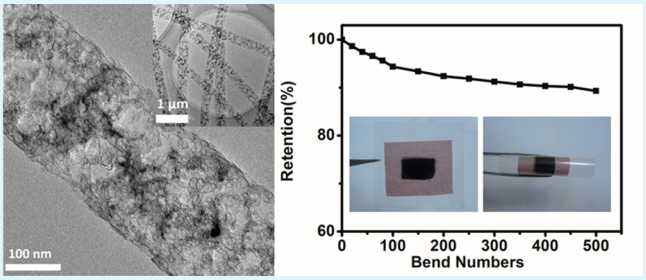

KEYWORDS: *porous carbon nanofibers, flexible, graphitization, electrospinning, supercapacitors*

INTRODUCTION

It is demonstrated that the performances of the electrochemical double layer capacitors (EDLCs) are greatly governed by the conductivity and specific surface area (SSA) of their electrode materials; especially, SSA usually determines the double-layer charging/discharging ability at the electrode/electrolyte interface.[1] Because of their high SSA, high conductivity, and high chemical stability, carbon nanomaterials, including graphene, carbon nanotubes (CNTs), and carbon nanofibers (CNFs), are frequently used for the electrodes of EDLCs.[2−5] Compared to graphene and CNT materials, the recent reported freestanding CNFs frameworks prepared by electrospinning technique show some advantages in preparation process, ion transmission, and cost, which is very crucial to real applications in supercapacitors.[6−8]

However, the SSA of electrospun CNFs (10−30 m^2 g^{-1}) is usually 1 order of magnitude lower than those of CNTs (272 m^2 g^{-1}) or graphene (909 m^2 g^{-1}).[2,8,9] It is known that porous materials usually possess a high SSA. Thus, in view of this point, many researchers have exploited various methods to synthesize porous carbon nanofibers (P-CNFs).[10−12] Jo et al.[7] used two types of polymers with different degrees of thermal stability to fabricate well-controlled P-CNFs, and the SSA of the prepared P-CNFs can reach 248.8 m^2 g^{-1}. Xia et al.[13] prepared ordered hierarchical porous carbon materials consisting of a type of 2D hexagonal mesostructures, which show a high surface area (1917 m^2 g^{-1}). This type of P-CNFs usually can exhibit a capacitance of 146 F g^{-1}, which is 3 times higher than that of the common CNFs.[8] Although the SSA of CNF materials has been greatly improved, most of those P-CNFs are often made of powder, which makes them need extra binders or conductive additives when assembled into electrodes, and initially leads to a great limitation in further improvement in their electrochemical performances. To overcome this drawback, Abeykoon et al.[14] have reported a type of binder-free P-CNF electrodes derived from immiscible PAN/PMMA polymer blends, which exhibits its highest surface area of 2419 m^2 g^{-1} and capacitance of 140 F g^{-1}. However, it is found that this paper did not pay attention to the flexibility of this type of freestanding P-CNFs frameworks and the sample exhibited a lower conductivity than graphene or CNTs,[15,16] which will greatly hinder their practical applications. More recently, researchers have tried to incorporate some conductive and flexible materials such as graphene and CNTs into CNFs to improve their flexibility and conductivity,[17,18] but it is still a challenge to prepare a type of flexible P-CNFs up until now.

Received: July 8, 2015
Accepted: October 9, 2015
Published: October 9, 2015

DOI: 10.1021/acsami.5b06107
ACS Appl. Mater. Interfaces 2015, 7, 23515−23520

Here, we reported a type of flexible and free-standing hierarchical P-CNF films fabricated by electrospinning technique combining with a subsequent metal etching process.[19−21] After carbonization process, this type of P-CNFs not only show a large SSA, but also exhibit a high flexibility and an improved conductivity, which are due to metal catalysis during thermal treatments. As designed, the P-CNFs show high specific capacitance, high rate-capability and high cycle stability. Moreover, the assembled devices show high flexibility and high mechanical stability. This research illustrates that this type of P-CNFs is a potential electrode materials for flexible energy storage, and might become one of the most promising candidates for all-carbon based supercapacitors.

EXPERIMENTAL SECTION

Materials. Hydrochloric acid (HCl), sulfuric acid (H_2SO_4), cobalt nitrate hexahydrate ($Co(NO_3)_2{\cdot}6H_2O$) were purchased from Alfa-Aesar Inc., USA; polyacrylonitrile (PAN, M_w ≈150 000) and polyvinylpyrrolidone (PVP, M_w ≈ 1 300 000) from Sigma-Aldrich Inc., USA; and N,N-dimethylformamide (DMF) from Tianjin Chemical Corp., Tianjin, China. All chemicals are analytical reagent. The H_2SO_4 was diluted to 0.5 M before using as the electrolyte, whereas the other chemicals were used as received without further purification.

Synthesis of P-CNFs. First, 0.6 g of PAN powder was dissolved in 6 mL of DMF. At the same time, 0.8 g of cobalt nitrate ($Co(NO_3)_2{\cdot}6H_2O$) and 0.75 g of PVP were dissolved in 4 mL of DMF. After being strongly stirred and becoming uniform, these two types of solutions were mixed together, followed by another stirring for 6 h. Then, the mixture solution was loaded into a 5 mL syringe for the electrospinning process, whose information can be reviewed in our previous work. The conditions of the electrospinning process were adjusted as follows: a trajectory distance of 20 cm, pump flow rate of 0.35 mL h^{-1}, and applied voltage of 12 kV. After electrospinning, the collected nanofiber films were first stabilized by heating up to 220 °C with rate of 2 °C min^{-1}, maintaining for 4 h under air flow. Then the samples were further heated at 350 °C for 4 h under an argon atmosphere. Subsequently, the samples were carbonized at 750 °C ∼ 800 °C for another 2 h under argon flow, respectively. Finally, the as-prepared cobalt−carbon composite films were clipped into pieces of 1 cm × 1.5 cm and immersed into 10 M HCl for 48 h to etch the cobalt nanoparticles. After being rinsed with deionized water for several times, P-CNFs were finally obtained. For comparison, the CNFs were synthesized by electrospinning the 10 wt % PAN solutions. Then, the CNFs were obtained after preoxidation and carbonization under the same process as the preparation of P-CNFs.

Structural Characterizations. Scanning electron microscope (SEM, Hitachi S-4800), transmission electron microscope (TEM, FEI Tecnai F30) were applied to analyze the structure and morphology of the materials. Raman spectra were recorded on a JY-HR800 micro-Raman spectrometer with a 532 nm laser as the excitation source. The X-ray photoelectron spectroscopy (XPS, PHI5702) was used to evaluate the elemental compositions. Nitrogen adsorption−desorption isothermals were measured at 77 K using Brunauer−Emmett−Teller (BET, ASAP2020, Micromeritics).

Electrochemical Measurements. Electrochemical tests (cyclic voltammetric (CV), electrochemical impedance (EIS) analysis, and galvanostatic charging−discharging (GCD) measurements) were performed on an Electrochemical Workstation (CS310, Wuhan Corrtest Instruments Co. Ltd., China) at ambient temperature.

The electrochemical tests were first performed using a three-electrode system, containing a platinum counter electrode, a SCE reference electrode, and the synthesized free-standing P-CNFs (0.77 mg) was used as working electrode, respectively. The electrolyte was a 0.5 M H_2SO_4 aqueous solution. The symmetric supercapacitors were built using two equal working electrode (0.6 mg) with a NKK separator and performed in a two-electrode system in 0.5 M H_2SO_4 (voltage range of 0−1.2 V). The energy storage properties of the P-CNFs based devices can be estimated using the following equations

$$C_M = (I\Delta t)/(M\Delta V) \quad (1)$$

$$E = 0.5C_M(\Delta V)^2 \quad (2)$$

$$P = E/\Delta t \quad (3)$$

Where C_M, I, Δt, M, and ΔV represents the specific capacitance (F g^{-1}) of the device, the discharge current (A), the discharge time (s), the total mass of electrode materials (g) and the device voltage (V) after the IR drop, respectively. E (Wh kg^{-1}) and P (W kg^{-1}) correspond to the energy density and power density of the device.[22]

RESULTS AND DISCUSSION

The schematic diagram in Figure 1a shows the preparation process of P-CNFs. The as-prepared electrospinning nanofibers

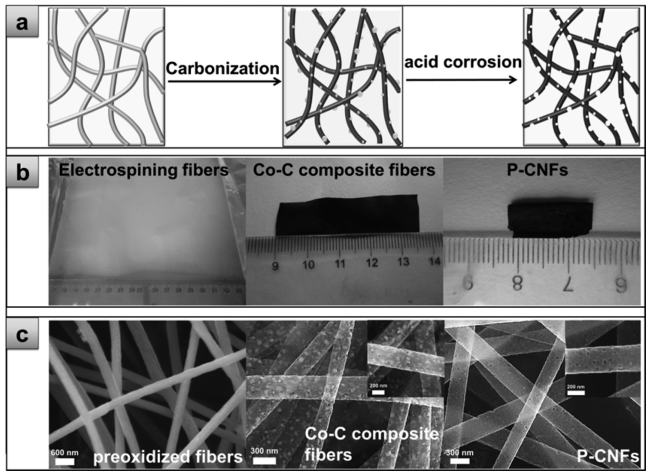

Figure 1. (a) Schematic illustration for the synthesis of P-CNFs by electrospining, carbonization and acid corrosion process. (b) The corresponding digital photographs of the electrospining fibers, the cobalt−carbon (Co−C) composite fibers and P-CNFs. (c) SEM images of the preoxidized fibers, the Co−C composite fibers (inset shows a single Co−C composite nanofiber) and P-CNFs (inset shows a single P-CNF).

were carbonized with proper temperature. During the carbonization process, the cobalt salt transformed into metal nanoparticles with different sizes; at the same time, the cobalt nanoparticles graphitize amorphous carbon into graphitic carbon. The cobalt nanoparticles were then leached with 10 M HCl. The HCl solution first etched the surface nanoparticles, then infiltrated into the internal of the fibers to react with the remained cobalt nanoparticles. HCl was properly chosen not only for its ability to dissolve cobalt nanoparticles but also for its inertness toward PAN macromolecules.[23] The obtained P-CNFs can provide interconnected channels for ions to migrate through the fibers and the inner pores, thus greatly decreasing the ions transport distance and transport resistance. Meanwhile, the graphitized carbon fibers can serve as the uninterrupted charge freeway networks for quick electron transfer.[24] Figure 1b showed the digital photographs of the electrospinning fibers, the Co−C composite fibers and P-CNFs, respectively, which correspond to the schematic diagram in Figure 1a. The morphology and structure of the preoxidized fibers, the Co−C composite fibers, and P-CNFs were examined by SEM, as shown in Figure 1c, the diameter of the samples is about 300 nm and distribute uniformly. It can be seen from the SEM

DOI: 10.1021/acsami.5b06107
ACS Appl. Mater. Interfaces 2015, 7, 23515−23520

image of the Co−C composite fibers that the cobalt nanoparticles distribute uniformly on the surface of the nanofibers. The low magnification SEM image of P-CNFs reveals that the cobalt nanoparticles were corroded completely and the magnified SEM image of P-CNFs clearly exhibit the porous structure of P-CNFs.

Cobalt salt was a key material for the formation of the unique hierarchical pore structure which acted as the porogen and catalyst. As shown in Figure 2a, the cobalt nanoparticles with

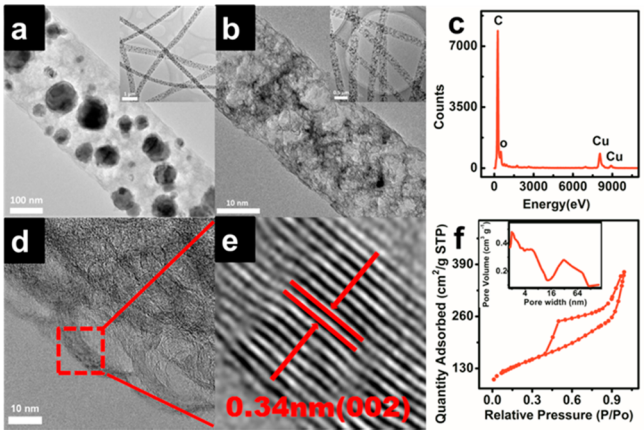

Figure 2. TEM image of (a) a single Co−C composite nanofiber (inset shows the low magnification TEM images) and (b) a single porous nanofibers, inset shows the low magnification TEM images of P-CNFs. (c) EDX spectrum of P-CNFs. (d) HTEM images of the porous nanofibers and (e) corresponding interplanar spacing. (f) Nitrogen sorption isotherms and pore size distribution of the P-CNFs (inset f).

different size distribute uniformly on the surface of the nanofibers. After these cobalt nanoparticles were leached by 10 M HCl, the obtained membrane is completely free-standing and flexible. Interestingly, without etching the cobalt nanoparticles, the composite nanofibers are very brittle. This enhanced mechanical property of the P-CNFs could be attributed to the unique hierarchical pore structure (Figure 2b), which could effectively release stress and avoid damage of P-CNFs during the bending.[6] To verify whether the cobalt nanoparticles were corroded completely, the EDX spectrum was tested as shown in Figure 2c, which reveal almost no residual cobalt. From the high-resolution TEM image of the porous nanofiber, onion-like structures appear around the pores (Figure 2d). These onionlike structures presenting circular dark fringes which correspond to curved carbon layers. The distance of the carbon layers is 0.34 nm which corresponding to the (002) plane of the carbon (Figure 2e). The onionlike structures catalyzed by cobalt nanoparticles present better crystallinity than the CNFs carbon fibers.[25] It is worth noting that doping the cobalt salt is not only beneficial to form the hierarchical pore structure but also to a better crystallization of the carbon components; this onionlike structure can also contribute to the enhanced mechanical property of the P-CNFs.

The porous structure and size distribution of P-CNFs were analyzed by Brunauer−Emmett−Teller (BET) measurements. The P-CNFs present a type-IV isotherm with H3 type hysteresis loop, showing the characteristics of a mesoporous material (Figure 2f). Moreover, the isotherm presents a sharp increase in the N_2 uptake at high relative pressures ($p/p_0 > 0.9$), indicating the existence of macropores in the sample.[26] The BET surface area of P-CNFs (468.9 $m^2 g^{-1}$) is much larger than that of the CNFs reported allowing an efficient contact of nanofibers with electrolyte. The corresponding pore size distribution curves (inset f) derived from the adsorption branch of the isotherm clearly shows the hierarchical pore structure. The micropores were generated during the preoxidation and carbonization process, which offer a good charge accommodation. However, the mesopores and macropores are contributed from removing the cobalt nanoparticles dispersed on the surface and embedded in the CNFs, which provide passageways for the icon to pass through.

The electrical resistance of P-CNFs was tested at the different bending angles which express little change for P-CNFs (Figure 3). Moreover, the P-CNFs fabricated in this paper

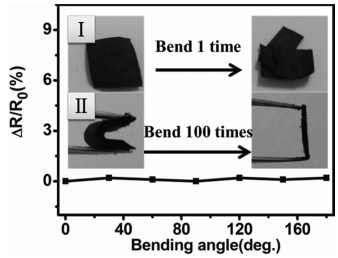

Figure 3. Electrical resistance for P-CNFs at the different bent angles, the inset shows the digital photographs of CNFs (I) and P-CNFs (II) bended after 100 times.

demonstrated excellent flexibility. As shown in inset, there is not any crack existing in P-CNFs (II) even after being bent 100 times, and it could recover to its initial state after releasing. By contrast, the CNFs (I) were brittle and becomes obviously damaged after being bent one time.

The characterization of P-CNFs by means of Raman scattering and X-ray photoelectron spectroscopy (XPS) is shown in Figure 4a, b. From Figure 4a, two feature peaks emerged at 1350 cm^{-1} (D band) and 1585 cm^{-1} (G band) could be observed for both samples. As is well-known, a typical D band resulting from the in-plane imperfections such as defects and heteroatoms of the graphitic lattice of the disordered sp^2-hybridized carbon, and a G band at 1585 cm^{-1} indicate the presence of crystalline graphitic carbon.[4] Compared with the CNFs carbon-fiber, both the D and G peaks of P-CNFs exhibit narrower and sharper peaks which implied more graphitic crystallites were present. The I_D/I_G of the P-CNFs is increased when compared with CNFs, which also indirectly proves that the formation of the pores can increase the defect of the fibers. XPS measurements could directly prove the graphitization degree of the fibers. The XPS survey spectrum for the P-CNFs showed a predominant narrow graphitic C 1s peak at 285 eV (Figure 4b). The absence of any Co peak on the survey spectrum indicates that the Co residues were completely removed by the HCl solution. As shown in the C 1s spectrum (Figure 4b), The two main peaks at 284.6 and 285.7 eV were assigned to sp^2-hybridized graphite-like carbon (C−C sp^2) and sp^3-hybridized diamond-like carbon (C−C sp^3), respectively. The peaks centered at 286.2, 287, and 289.1 eV were attributed to surface oxygen groups (designated as C−O, C═O, and O═C−O, respectively).[27]

The electrochemical capacitive performances of P-CNFs were evaluated by cyclic voltammetry (CV) and galvanostatic charge/discharge (GCD) measurement. Figure 5a shows the

DOI: 10.1021/acsami.5b06107
ACS Appl. Mater. Interfaces 2015, 7, 23515−23520

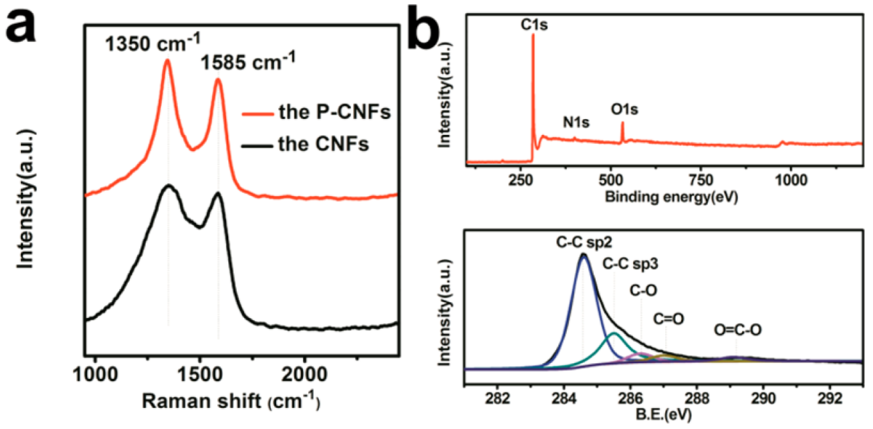

Figure 4. (a) Raman spectras of porous nanofibers and the CNFs. (b) XPS spectra of porous nanofibers and C 1s spectrum.

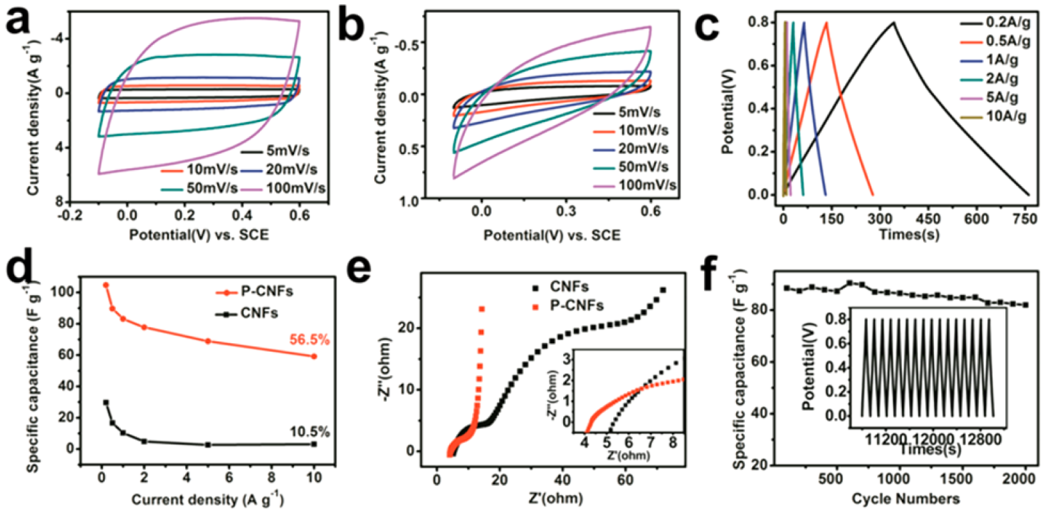

Figure 5. CV curves of (a) P-CNFs and (b) the CNFs at varied potential scan rates (5−100 mV s^{-1}). (c) GCD curves of the P-CNFs at different current densities (0.5−10 A g^{-1}). (d) Gravimetric capacitance as a function of current density (e) Nyquist plots of P-CNFs and the CNFs electrodes measured with amplitude of 10 mV over the frequency range from 100000 to 0.1 Hz, inset: the magnified high frequency region. (f) Cycle performance of P-CNFs at 1 A g^{-1} over 2000 cycles and the last 20 charge/discharge curves (inset f).

CV curves of the P-CNFs at scan rates of 5, 10, 20, 50, and 100 mV s^{-1} with a potential window ranging from −0.1 to 0.6 V in 0.5 M H_2SO_4 solution. At the high scan rates of 100 mV s^{-1}, the CV profiles of the samples maintain the rectangular shape of the voltammograms with little distortion, which can be attributed to the excellent electrical conductivity and the low mass-transport resistance of the samples. On the contrary, The CV curves of CNFs at varied potential scan rates showed a strong polarization phenomenon and a much smaller area (Figure 5b). These results can be attributed to the low conductivity and hydrophobicity of the CNFs. Four probe measurements indicated the average square resistance of the CNFs is ∼261.3 Ω/□ but the average square resistance of P-CNFs is ∼155.5 Ω/□. Figure 5c shows the GCD curves of P-CNFs at different current densities (0.2−10 A g^{-1}), the specific capacitance is up to 104 F g^{-1}. Rate capability of P-CNFs and CNFs are depicted in Figure 5d, the specific capacitances of both samples decreased as the current density increased, when increase the current density to 10 A g^{-1}, the capacitance retention of P-CNFs is 56.5%, while the retention of CNFs under the same current density is only 10.5%. The enhancement of the rate capability of the P-CNFs is mainly attributed to the improved conductivity which facilitating the electron transportation, resulting in a faster electronic response.

The Nyquist plots (Figure 5e) of the samples are characterized by a semicircle at high frequency and a sharp increase in the imaginary part of the impedance at lower frequency. In the high frequency range, the left plot intersection at real part (Z') is associated with the electrolyte resistance (R_s) and the square resistance of the samples (inset e). The semicircle region in the plot curve corresponds to the charge transfer resistance (R_{ct}), which indicates the migration rate of ions at the interface between the solution and the electrode surface. Meanwhile, the smaller diameter of semicircle in the EIS spectrum of P-CNFs has an indication of lower charge-transfer resistance. In the low frequency region, this line has a finite slope representing the diffusive resistivity of the electrolyte within the pore of the electrode, as represented by Warbug impedance. The slope of the P-CNFs approached to an ideally straight line implying the enhanced accessibility of the ions.[28] To investigate the cycling stability of the P-CNFs, we performed GCD tests at a current density of 1 A g^{-1} (Figure 5f). The results demonstrate that the specific capacitance of P-CNFs retained about 94% after 2000 charging/discharging cycles. All these results reveal that this type of porous

DOI: 10.1021/acsami.5b06107
ACS Appl. Mater. Interfaces 2015, 7, 23515−23520

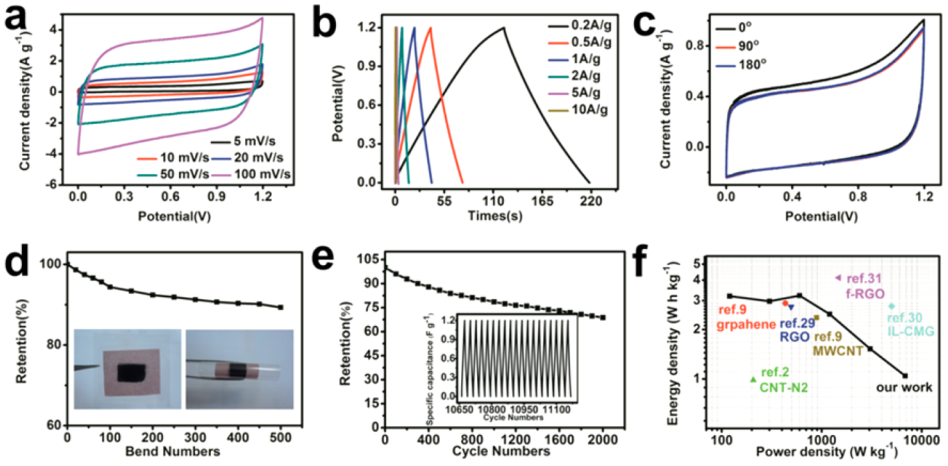

Figure 6. Electrochemical performance of P-CNFs measured in a two-electrode system. (a) CV curves at varied sweep rate increasing from 5 to 100 mV s^{-1}. (b) GCD curves; (c) CV curves of the symmetrical supercapacitors bent with different angles at sweep rate of 10 mV s^{-1}. (d) Capacitance retention of the symmetrical supercapacitors for bending cycles, inset shows digital photographs of the flexibility of the device during releasing and bending operations. (e) Cycle performance of the devices at 1 A g^{-1} over 2000 cycles and the last 20 charge/discharge curves (inset e). (f) Ragone plots of the flexible supercapacitors, compared with the values of similar symmetrical systems from refs 2, 9, and 29−31. Reproduced with permission from ref 29. Copyright 2011 Royal Society of Chemistry. Reproduced with permission from ref 30. Copyright 2012 Royal Society of Chemistry. Reproduced with permission from ref 31. Copyright 2015 IOP publisher.

nanostructure and high graphitization degree of the P-CNFs could facilitate the electrolyte ion diffusion and electron transportation, leading to a reduced internal resistance and an improved electrochemical performance.

Furthermore, two-electrode symmetrical supercapacitors were also carried out to evaluate electrochemical performance of P-CNFs with 0.5 M H_2SO_4 as electrolyte. Figure 6a shows the CV curves of symmetrical device based on P-CNFs at different sweep rates ranging from 5 to 100 m V s^{-1} in voltage window of 0−1.2 V. It can be found that the CV curves can retain rectangular shape with the sweep rate reaches up to 100 mV s^{-1}. The GCD curves (Figure 6b) exhibits nearly triangular shape without obvious *IR* drop at a current density of 2 A g^{-1}, suggesting a high reversibility of a typical capacitor with a rapid *I*−*V* response because of its improved graphitization degree which could enhance the electrical conductivity.[6] To further explore the advantage of flexible P-CNFs, we also performed CV and GCD measurements on the supercapacitors upon bending at different angles and times. As illustrated in Figure 6c, no obvious change of CV curves at 10 mV s^{-1} can be observed when the device was even bent to 180°. The bending cycles of the device was also tested, as shown in Figure 6d, the resulting specific capacitance retained 89.4% of its initial value even after 500 bending cycles, indicating its excellent mechanical and flexible properties. Inset d exhibits the flexibility of the device. GCD technique was also performed to evaluate the cycling stability of this symmetric supercapacitors at 1 A g^{-1} current density (Figure 6e), the results demonstrate that the charge/discharge capacitance retain 69.0% after 2000th cycles. The Ragone plot (energy density versus average power density) is presented in Figure 6f, the energy density and the power density can be estimated using the aforementioned equations. P-CNFs could deliver a high energy density of 3.22 Wh kg^{-1} with a power density of 600 W kg^{-1}. This value is higher than that of other carbon based aqueous supercapacitors, such as MWCNT film (2.4 Wh kg^{-1} at a power density of 900 W kg^{-1}), graphene film (2.94 Wh kg^{-1} at a power density of 438.6 W kg^{-1}), CNT-N2 (1.0 Wh kg^{-1} at a power density of 210 W kg^{-1}).[2,9,29−31] This further demonstrates that the formation of hierarchical pore structures could effectively improve the power density of the device.

CONCLUSION

In summary, we have successfully designed and synthesized flexible and highly graphitized P-CNFs that can provide fast ion-diffusion and electron-transfer channels for supercapacitors applications. The electrode show effective improved cycling stability, the specific capacitance of P-CNFs retained about 94% after 2000 charging/discharging cycles and the capacitance retaind 89.4% after 500 bending cycles, these remarkable performances might be attributed to the high graphitization degree and the unique hierarchical pore structures of the sample. With flexible, hierarchical pores and high conductive features, this unique structure of P-CNFs represents great potential in the development of flexible energy storage system and can serve as good scaffold to support capacitive active materials.

AUTHOR INFORMATION

Corresponding Authors

*E-mail: xjpan@lzu.edu.cn. Tel.: +86 931 8912626. Fax: +86 931 8913554.

*E-mail: xieeq@lzu.edu.cn.

Notes

The authors declare no competing financial interest.

ACKNOWLEDGMENTS

We acknowledge the financial support by the National Natural Science Foundation of China (11474135, U1232121, and 51202100) and the Fundamental Research Funds for the Central Universities (lzujbky-2015-110).

REFERENCES

(1) Zhai, Y.; Dou, Y.; Zhao, D.; Fulvio, P. F.; Mayes, R. T.; Dai, S. Carbon Materials for Chemical Capacitive Energy Storage. *Adv. Mater.* **2011**, *23* (42), 4828−4850.

(2) Sevilla, M.; Yu, L.; Zhao, L.; Ania, C. O.; Titiricic, M.-M. Surface Modification of CNTs with N-Doped Carbon: An Effective Way of

DOI: 10.1021/acsami.5b06107
ACS Appl. Mater. Interfaces 2015, 7, 23515−23520

Enhancing Their Performance in Supercapacitors. *ACS Sustainable Chem. Eng.* **2014**, *2* (4), 1049−1055.
(3) Xiao, X.; Peng, X.; Jin, H.; Li, T.; Zhang, C.; Gao, B.; Hu, B.; Huo, K.; Zhou, J. Freestanding Mesoporous VN/CNT Hybrid Electrodes for Flexible All-Solid-State Supercapacitors. *Adv. Mater.* **2013**, *25* (36), 5091−5097.
(4) Zhou, W.; Zhou, K.; Liu, X.; Hu, R.; Liu, H.; Chen, S. Flexible Wire-Like All-Carbon Supercapacitors Based On Porous Core−Shell Carbon Fibers. *J. Mater. Chem. A* **2014**, *2* (20), 7250−7255.
(5) Meng, Y.; Wang, K.; Zhang, Y.; Wei, Z. Hierarchical Porous Graphene/Polyaniline Composite Film with Superior Rate Performance for Flexible Supercapacitors. *Adv. Mater.* **2013**, *25* (48), 6985−6990.
(6) Cheng, Y.; Huang, L.; Xiao, X.; Yao, B.; Yuan, L.; Li, T.; Hu, Z.; Wang, B.; Wan, J.; Zhou, J. Flexible and Cross-Linked N-Doped Carbon Nanofiber Network for High Performance Freestanding Supercapacitor Electrode. *Nano Energy* **2015**, *15*, 66−74.
(7) Jo, E.; Yeo, J.-G.; Kim, D. K.; Oh, J. S.; Hong, C. K. Preparation of Well-Controlled Porous Carbon Nanofiber Materials by Varying the Compatibility of Polymer Blends. *Polym. Int.* **2014**, *63* (8), 1471−1477.
(8) Pan, H.; Yang, J.; Wang, S.; Xiong, Z.; Cai, W.; Liu, J. Facile Fabrication of Porous Carbon Nanofibers by Electrospun PAN/Dimethyl Sulfone for Capacitive Deionization. *J. Mater. Chem. A* **2015**, *3*, 13827−13834.
(9) Li, N.; Yang, G.; Sun, Y.; Song, H.; Cui, H.; Yang, G.; Wang, C. Free-Standing and Transparent Graphene Membrane of Polyhedron Box-Shaped Basic Building Units Directly Grown Using a NaCl Template for Flexible Transparent and Stretchable Solid-State Supercapacitors. *Nano Lett.* **2015**, *15* (5), 3195−3203.
(10) He, H.; Shi, L.; Fang, Y.; Li, X.; Song, Q.; Zhi, L. Mass Production of Multi-Channeled Porous Carbon Nanofibers and Their Application as Binder-Free Electrodes for High-Performance Supercapacitors. *Small* **2014**, *10* (22), 4671−4676.
(11) Barranco, V.; Lillo-Rodenas, M. A.; Linares-Solano, A.; Oya, A.; Pico, F.; Iban, J.; Agullo-Rueda, F.; Amarilla, J. M.; Rojo, J. M. Amorphous Carbon Nanofibers and Their Activated Carbon Nanofibers as Supercapacitor Electrodes. *J. Phys. Chem. C* **2010**, *114* (22), 10302−10307.
(12) Wang, Y.; Xia, Y. Recent Progress in Supercapacitors: From Materials Design to System Construction. *Adv. Mater.* **2013**, *25* (37), 5336−5342.
(13) Liu, H.-J.; Wang, J.; Wang, C.-X.; Xia, Y.-Y. Ordered Hierarchical Mesoporous/Microporous Carbon Derived from Mesoporous Titanium-Carbide/Carbon Composites and its Electrochemical Performance in Supercapacitor. *Adv. Energy Mater.* **2011**, *1* (6), 1101−1108.
(14) Abeykoon, N. C.; Bonso, J. S.; Ferraris, J. P. Supercapacitor Performance of Carbon Nnanofiber Electrodes Derived from Immiscible PAN/ PMMA Polymer Blends. *RSC Adv.* **2015**, *5*, 19865−19873.
(15) Frackowiak, E.; Metenier, K.; Bertagna, V.; Beguin, F. Supercapacitor Electrodes from Multiwalled Carbon Nanotubes. *Appl. Phys. Lett.* **2000**, *77* (15), 2421−2423.
(16) Zhai, T.; Lu, X.; Wang, H.; Wang, G.; Mathis, T.; Liu, T.; Li, C.; Tong, Y.; Li, Y. An Electrochemical Capacitor with Applicable Energy Density of 7.4 Wh/kg at Average Power Density of 3000 W/kg. *Nano Lett.* **2015**, *15* (5), 3189−3194.
(17) Cheng, Y.; Lu, S.; Zhang, H.; Varanasi, C. V.; Liu, J. Synergistic Effects from Graphene and Carbon Nanotubes Enable Flexible and Robust Electrodes for High-Performance Supercapacitors. *Nano Lett.* **2012**, *12* (8), 4206−4211.
(18) Qian, X.; Lv, Y.; Li, W.; Xia, Y.; Zhao, D. Multiwall Carbon Nanotube@Mesoporous Carbon with Core-Shell Configuration: a Well-Designed Composite-Structure toward Electrochemical Capacitor Application. *J. Mater. Chem.* **2011**, *21* (34), 13025−13031.
(19) Kim, C.; Ngoc, B. T. N.; Yang, K. S.; Kojima, M.; Kim, Y. A.; Kim, Y. J.; Endo, M.; Yang, S. C. Self-Sustained Thin Webs Consisting of Porous Carbon Nanofibers for Supercapacitors via the Electrospinning of Polyacrylonitrile Solutions Containing Zinc Chloride. *Adv. Mater.* **2007**, *19* (17), 2341−2346.
(20) Nataraj, S. K.; Kim, B. H.; dela Cruz, M.; Ferraris, J.; Aminabhavi, T. M.; Yang, K. S. Free Standing Thin Webs of Porous Carbon Nanofibers of Polyacrylonitrile Containing Iron-Oxide by Electrospinning. *Mater. Lett.* **2009**, *63* (2), 218−220.
(21) Nataraj, S. K.; Kim, B. H.; Yun, J. H.; Lee, D. H.; Aminabhavi, T. M.; Yang, K. S. Effect of Added Nickel Nitrate on the Physical, Thermal and Morphological Characteristics of Polyacrylonitrile-Based Carbon Nanofibers. *Mater. Sci. Eng., B* **2009**, *162* (2), 75−81.
(22) Long, C.; Jiang, L.; Wu, X.; Jiang, Y.; Yang, D.; Wang, C.; Wei, T.; Fan, Z. Facile Synthesis of Functionalized Porous Carbon with Three-Dimensional Interconnected Pore Structure for High Volumetric Performance Supercapacitors. *Carbon* **2015**, *93*, 412−420.
(23) Mehraban, M.; Zadhoush, A.; Ravandi, S. A. H.; Bagheri, R.; Tehrani, A. H. Preparation of Porous Nanofibers from Electrospun Polyacrylonitrile/Calcium Carbonate Composite Nanofibers Using Porogen Leaching Technique. *J. Appl. Polym. Sci.* **2013**, *128* (2), 926−933.
(24) He, Y.; Chen, W.; Zhou, J.; Li, X.; Tang, P.; Zhang, Z.; Fu, J.; Xie, E. Constructed Uninterrupted Charge-Transfer Pathways in Three-Dimensional Micro/Nanointerconnected Carbon-Based Electrodes for High Energy-Density Ultralight Flexible Supercapacitors. *ACS Appl. Mater. Interfaces* **2014**, *6* (1), 210−218.
(25) Chen, Y.; Li, X.; Zhou, X.; Yao, H.; Huang, H.; Mai, Y.-W.; Zhou, L. Hollow-Tunneled Graphitic Carbon Nanofibers through Ni-Diffusion-Induced Graphitization as High-Performance Anode Materials. *Energy Environ. Sci.* **2014**, *7* (8), 2689−2696.
(26) Fan, Y.; Yang, X.; Zhu, B.; Liu, P.-F.; Lu, H.-T. Micro-Mesoporous Carbon Spheres Derived from Carrageenan as Electrode Material for Supercapacitors. *J. Power Sources* **2014**, *268*, 584−590.
(27) Zhang, L.; Su, Z.; Jiang, F.; Yang, L.; Qian, J.; Zhou, Y.; Li, W.; Hong, M. Highly Graphitized Nitrogen-Doped Porous Carbon Nanopolyhedra Derived from ZIF-8 Nanocrystals as Efficient Electrocatalysts for Oxygen Reduction Reactions. *Nanoscale* **2014**, *6*, 6590−6602.
(28) Kim, C.; Yang, K. S. Electrochemical Properties of Carbon Nanofiber Web as an Electrode for Supercapacitor Prepared by Electrospinning. *Appl. Phys. Lett.* **2003**, *83* (6), 1216−1218.
(29) Zhang, J.; Jiang, J.; Li, H.; Zhao, X. S. A High-Performance Asymmetric Supercapacitor Fabricated with Graphene-Based Electrodes. *Energy Environ. Sci.* **2011**, *4* (10), 4009−4015.
(30) Choi, B. G.; Chang, S. J.; Kang, H. W.; Park, C. P.; Kim, H. J.; Hong, W. H.; Lee, S.; Huh, Y. S. High Performance of a Solid-State Flexible Asymmetric Supercapacitor Based On Graphene Films. *Nanoscale* **2012**, *4* (16), 4983−4988.
(31) Luo, Q. P.; Huang, L.; Gao, X.; Cheng, Y.; Yao, B.; Hu, Z.; Wan, J.; Xiao, X.; Zhou, J. Activated Carbon Derived from Melaleuca Barks for Outstanding High-Rate Supercapacitors. *Nanotechnology* **2015**, *26* (30), 304004.

DOI: 10.1021/acsami.5b06107
ACS Appl. Mater. Interfaces 2015, 7, 23515−23520